APL Materials

Stabilization of ferroelectric $Hf_xZr_{1-x}O_2$ films using a millisecond flash lamp annealing technique

Cite as: APL Mater. **6**, 121103 (2018); https://doi.org/10.1063/1.5060676
Submitted: 21 September 2018 . Accepted: 23 November 2018 . Published Online: 11 December 2018

Éamon O'Connor, Mattia Halter, Felix Eltes, Marilyne Sousa, Andrew Kellock, Stefan Abel, and Jean Fompeyrine

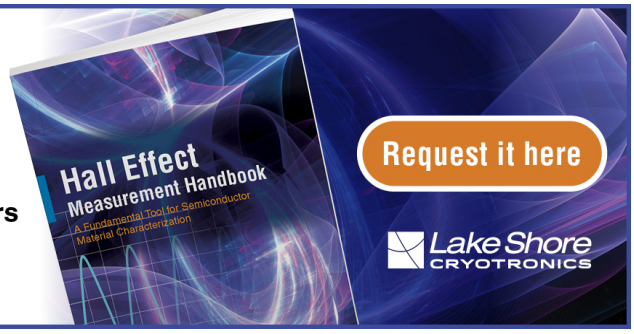

Stabilization of ferroelectric $Hf_xZr_{1-x}O_2$ films using a millisecond flash lamp annealing technique

Éamon O'Connor,[1,a] Mattia Halter,[1,2] Felix Eltes,[1] Marilyne Sousa,[1] Andrew Kellock,[3] Stefan Abel,[1] and Jean Fompeyrine[1]
[1]*IBM Research GmbH—Zurich Research Laboratory, Säumerstrasse 4, CH-8803 Rüschlikon, Switzerland*
[2]*Integrated Systems Laboratory, Swiss Federal Institute of Technology Zurich, CH-8092 Zurich, Switzerland*
[3]*IBM Almaden Research Center, 650 Harry Rd., San Jose, California 95120, USA*

(Received 21 September 2018; accepted 23 November 2018; published online 11 December 2018)

We report on the stabilization of ferroelectric $Hf_xZr_{1-x}O_2$ (HZO) films crystallized using a low thermal budget millisecond flash lamp annealing technique. Utilizing a 120 s 375 °C preheat step combined with millisecond flash lamp pulses, ferroelectric characteristics can be obtained which are comparable to that achieved using a 300 s 650 °C rapid thermal anneal. X-ray diffraction, capacitance voltage, and polarization hysteresis analysis consistently point to the formation of the ferroelectric phase of HZO. A remanent polarization (P_r) of ~21 $\mu C/cm^2$ and a coercive field (E_c) of ~1.1 MV/cm are achieved in 10 nm thick HZO layers. Such a technique promises a new alternative solution for low thermal budget formation of ferroelectric HZO films. https://doi.org/10.1063/1.5060676

HfO_2 based ferroelectric films have become of increased interest in recent years since the report of ferroelectricity in the HfO_2 material system by Böscke *et al.*[1] They offer advantages over more traditional ferroelectrics, such as perovskites, due to a variety of factors, among them improved scaling potential and superior CMOS process compatibility.[2,3] Ferroelectricity has been observed by incorporating a number of different dopant atoms in HfO_2, among them Si,[1] Y,[4] Gd,[5] Sr,[6] and La.[7] $Hf_xZr_{1-x}O_2$ (HZO) films have emerged as one of the more promising ferroelectric material candidates.[8] This in part is due to the fact that there is a wider and more forgiving composition window where ferroelectricity is observed in mixed HfO_2 and ZrO_2 films than that for doped HfO_2 films. One of the most critical aspects in respect of HZO and other doped HfO_2 films is to control the temperature profile of the crystallization anneal. It is essential to form and stabilize the metastable, non-centrosymmetric orthorhombic phase, which is considered responsible for the ferroelectric behavior observed in these films.[2,9] Temperatures in the range of 400 °C–800 °C have been reported in the literature for formation of ferroelectric HZO films.[8,10–13] In this work, we report on HZO films where ferroelectric behavior is demonstrated using a millisecond flash lamp annealing (FLA) process. This technique involves pre-heating a sample at an intermediate temperature prior to the delivery of an energy pulse of millisecond duration using an array of xenon flash lamps.[14] In applying such a technique, the HZO films can therefore be pre-heated below their crystallization temperature and the final temperature required for formation of the ferroelectric phase is achieved using an energy pulse on a millisecond time scale. This offers a promising approach in terms of reduced thermal budget requirements for processing of such ferroelectric films.

Highly doped Si substrates were dipped in buffered hydrofluoric acid (BHF, 7:1) for ~20 s to remove the native oxide prior to immediate transfer to an Oxford Instruments plasma enhanced atomic layer deposition (PEALD) system. Initially ~10 nm TiN was deposited using a

[a]Currently at EPFL, Lausanne, Switzerland.

tetrakis(dimethylamino)titanium (TDMAT) precursor and N_2/H_2 plasma. Approximately 10 nm thick layers of HZO were grown in a process using alternating cycles of tetrakis(ethylmethylamino)hafnium (TEMAH) and ZrCMMM ((MeCp)2Zr(OMe) (Me)). Rutherford Back Scattering (RBS) analysis of the films (not shown) indicated an actual film composition of $Hf_{0.57}Zr_{0.43}O_2$. A further 10 nm of TiN was immediately deposited *in situ* in the PEALD. All anneals were performed prior to PVD deposition of 100 nm W to form top contacts for the metal-insulator-metal (MIM) structures. Metal gate patterning and etch was performed using standard UV lithography and fluorine-based reactive ion etch processes. Capacitance voltage (CV), polarization versus electric field (PE), positive up negative down (PUND), and leakage characterization were performed on the resulting MIM structures, which have an area of $50 \times 50\ \mu m^2$. CV curves were obtained using an Agilent B1500 parameter analyzer, while the PE loops, PUND, and leakage were measured using a TF Analyzer 2000 from AixAct. Grazing incidence X-ray diffraction (GIXRD) measurements were performed in a Bruker D8 Discover diffractometer equipped with a rotating anode generator. Bright field STEM (BF-STEM) measurements were performed using a double spherical aberration-corrected JEOL JEM-ARM200F microscope operated at 200 kV.

The Flash Lamp Anneal (FLA) tool layout consists of a xenon flash lamp array located at the top of the chamber in addition to a conventional halogen lamp heater located under the sample holder for the pre-heat step.[14] The actual temperature reached during the millisecond flash lamp anneal (*ms-FLA*) depends on the initial pre-heat temperature, and the energy and duration of the flash pulse, both of which can be varied. Pulse durations in the range of 0.3–20 ms can be performed, where this duration refers to the full-width at half-maximum of the energy pulse. Energy density values up to 110 J/cm^2 are possible in this flash anneal tool. For the samples in the current study, the preheat conditions were 120 s at 375 °C, while the flash duration was maintained at 20 ms, and the flash energy was varied. While the pre-heating was monitored via thermocouple control, there is no facility to monitor the temperature spike during the flash. The actual energy absorbed by a sample during a flash annealing process will be dependent on the material structure of the sample. For comparison, a sample was also prepared in the same chamber where regular rapid thermal annealing (*RTA*) was performed at 650 °C for 300 s with no *ms-FLA* step.

Figure 1 shows transmission electron microscopy (TEM) cross sections of the MIM devices. Figure 1(a) shows a micrograph of the full W/TiN/HZO/TiN/n$^+$Si MIM structure. The TEM analysis confirms the thicknesses of the TiN layers (~10 nm) and of the HZO layer (~10 nm). The various layers are clearly uniform with low roughness at the interfaces. Figures 1(b) and 1(c) show more scaled micrographs focusing on the TiN/HZO/TiN stack, for the sample which received a regular 300 s 650 °C *RTA* with no flash anneal step, and the 70 J/cm^2 *ms-FLA* sample, respectively. The TEM images show a similar microstructure and confirm the polycrystalline nature of the TiN electrodes and the HZO layer in both cases. Therefore it is clear that the 120 s preheat at 375 °C combined with 70 J/cm^2 *ms-FLA* is sufficient to fully crystallize the 10 nm HZO layer.

The GIXRD results are exhibited in Fig. 2 where the range of the diffraction angle (2θ) is limited to 28°–34°. In this region, one can easily distinguish between the non-ferroelectric monoclinic phase and the cubic, tetragonal, or orthorhombic phase, only the latter one being ferroelectric. A reference

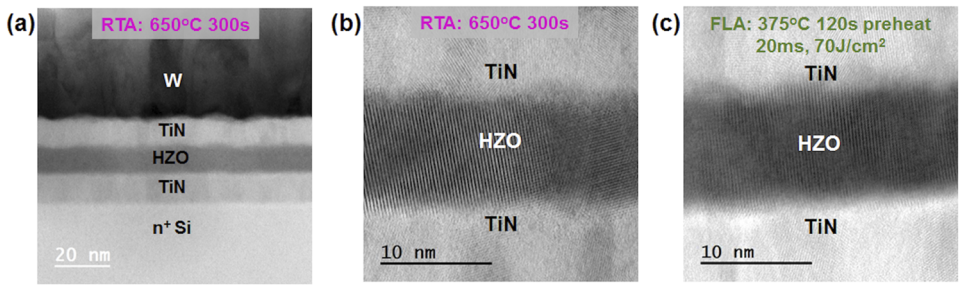

FIG. 1. (a) TEM cross section of the W/TiN/HZO/TiN/n$^+$Si MIM structure. The TEM micrographs in (b) and (c) focus on the TiN/HZO/TiN layers for the 300 s 650 °C *RTA* sample and the 70 J/cm^2 *ms-FLA* sample, respectively.

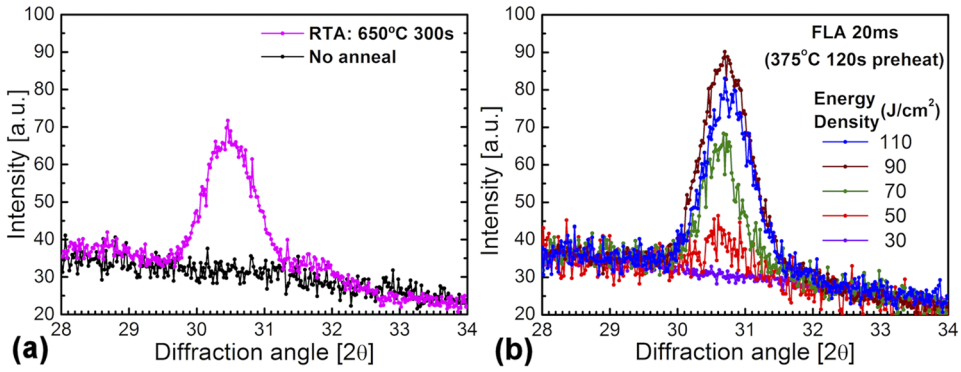

FIG. 2. (a) GIXRD for a diffraction angle (2θ) from 28° to 34° for a reference sample which received no anneal and a sample which received a regular 300 s 650 °C *RTA*. (b) GIXRD profiles for the millisecond flash lamp annealed samples with a varying flash energy density of 20 ms duration. In each case, there was a 120 s preheat step at 375 °C.

sample which received no anneal did not exhibit peaks in this region; as seen in Fig. 2(a). The sample which received a regular 300 s 650 °C *RTA* step has a peak centered around 30.5° which can be assigned to tetragonal and/or orthorhombic phases in HZO although distinguishing them from each other is difficult using XRD owing to their very similar structure.[10] However it provides promising structural evidence for the possible existence of the orthorhombic phase responsible for ferroelectric behavior in HZO films.[8] The XRD profiles for the millisecond flash lamp annealed samples with a varying flash energy of 20 ms duration are shown in Fig. 2(b). In each case, there was a 120 s preheat step at 375 °C. For the 110, 90, and 70 J/cm^2 *ms-FLA* samples, a peak is observed in the XRD around 30.5°, with the magnitude reducing slightly for the 70 J/cm^2 sample. When the flash energy is reduced to 50 J/cm^2, this peak magnitude is significantly diminished, while at 30 J/cm^2, it is not evident. The XRD profiles for the other *ms-FLA* samples are similar to that recorded in Fig. 2(a) for the 300 s 650 °C *RTA* sample, indicating the possible presence of the non-centrosymmetric orthorhombic phase required for ferroelectricity.

Figure 3 shows capacitance voltage curves measured at 10 kHz for MIM structures for all anneal conditions in the current study and which had been subjected to electric field cycling prior to measurement (~1500 cycles). For the unannealed sample in Fig. 3(a), no peaks are observed in the CV which is expected for a non-ferroelectric film. By contrast, the sample which received a regular 300 s 650 °C *RTA* step in Fig. 3(b) displays butterfly shaped CV hysteresis curves consistent with

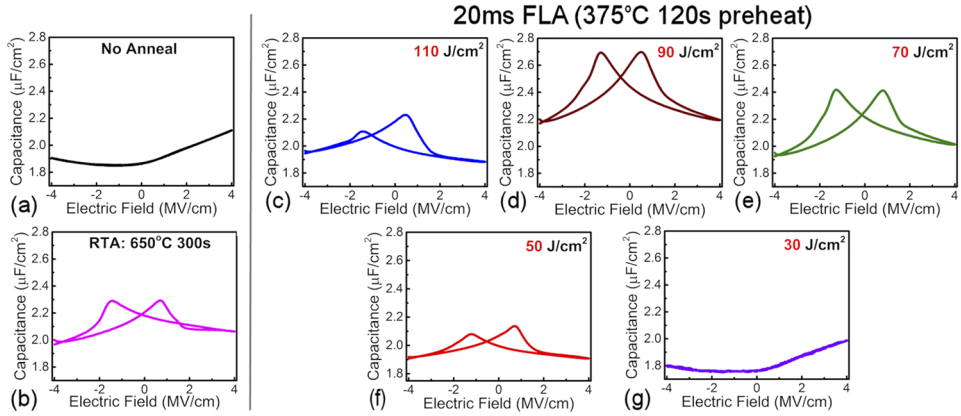

FIG. 3. Capacitance voltage characteristics measured on W/TiN/HZO/TiN/n$^+$Si MIM structures at room temperature with a small signal AC frequency of 10 kHz and an amplitude of 50 mV. The left panel shows CVs for (a) the unannealed sample and (b) the 300 s 650 °C *RTA* sample with no flash anneal. The right panel [(c)–(g)] shows the CVs for the millisecond flash annealed samples with varying flash pulse energy. In each case, there was a 120 s preheat step at 375 °C and the flash pulse duration was 20 ms.

that reported previously for ferroelectric HZO.[11,12] The CVs for the various *ms-FLA* samples are displayed in the right hand panel of Fig. 3. The 110 J/cm^2 sample exhibits a non-linear CV response. A more prominent and symmetric butterfly shaped CV curve is observed for the 90 J/cm^2 and 70 J/cm^2 samples, while this is reduced again for the 50 J/cm^2 sample. However, the 30 J/cm^2 sample is almost identical to that of the unannealed film, providing further evidence along with the XRD analysis that this energy pulse is too low for crystallization of the ferroelectric phase in HZO. Furthermore this is indicative that the sample pre-heat step (375 °C for 120 s) is insufficient for formation of the orthorhombic phase in these films. In terms of the CV behavior, the 70 J/cm^2 *ms-FLA* sample most closely resembles the characteristics of the 300 s 650 °C *RTA* sample.

A real-time measurement of the temperature spike during the millisecond flash anneal process is not trivial and beyond the scope of the present experimental setup. As stated earlier, the temperature increase is obviously dependent on the flash energy and the thickness and composition of the materials incorporated in the device structure. Given the similarity in XRD and CV characteristics for the 300 s 650 °C *RTA* with no flash anneal step and the sample subjected to 70 J/cm^2 *ms-FLA* with 120 s 375 °C preheat, we estimate that a temperature increase in the range of 200 °C–300 °C is likely for this flash condition. The spectral output of the xenon lamps used in this tool is broad extending from ~300 nm to 950 nm, similar to that reported by Skorupa *et al.*[14] The HZO films in the current study were flash annealed after top TiN deposition. Given that HZO is transparent above ~250 nm[15] and that absorption spectra reported for TiN[16,17] and silicon[18] overlap with the spectral output emitted by the xenon flash lamps, we surmise that radiant energy from the millisecond flash is absorbed in the TiN or silicon and transferred to the HZO layer. The reflectivity of the TiN and Si must also be taken into account. Some modeling and simulation is likely required[18] to comprehensively understand the precise mechanisms and contributions of the layers in the current structure for crystallization of the HZO during millisecond flash anneal, and this is subject to further investigation.

Polarization versus electric field (PE) characterization was performed on the MIM structures to investigate hysteretic behavior of the HZO films. Figure 4 exhibits PE hysteresis loops measured at 1 kHz and at room temperature for all samples. For each sample, the PE loop on a pristine device is plotted along with the PE loop obtained after electric field cycling of the same devices.[19] As seen in Fig. 4(a), the sample which received no annealing step, and which exhibited no orthorhombic peak in the XRD analysis, and no peaks in the CV displays a negligible hysteresis and linear PE characteristic, as would be expected for the non-ferroelectric material.[10] Likewise the linear PE loop in Fig. 4(b) for the 30 J/cm^2 *ms-FLA* sample indicates the absence of ferroelectricity which is similarly consistent with the XRD and CV data shown earlier. All other samples measured in a pristine state show pinched PE hysteresis loops. This is significantly improved by post cycling in all cases, with the stressing enhancing both positive and negative remanent polarization. This is in agreement with the so-called

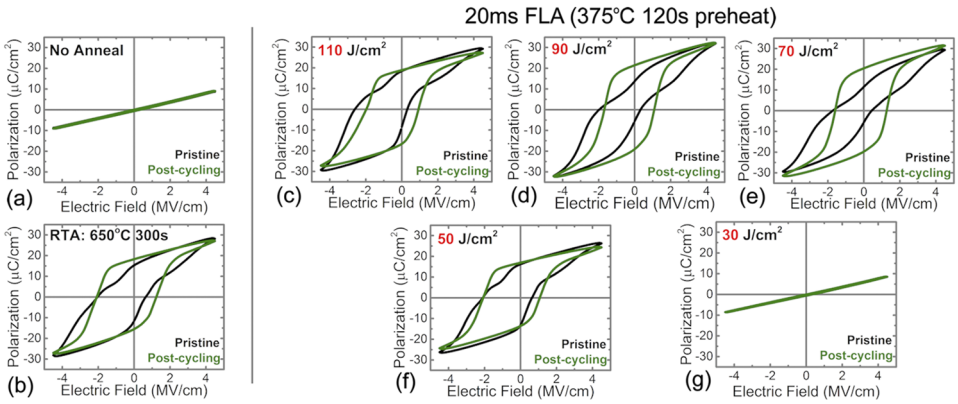

FIG. 4. Polarization versus electric field (PE) characteristics measured on W/TiN/HZO/TiN/n$^+$Si MIM structures at room temperature and at 1 kHz. Hysteresis loops are shown for each sample both in pristine condition and post electric field cycling (~1500 cycles). The left panel shows PE hysteresis loops for (a) the unannealed sample and (b) the 300 s 650 °C *RTA* sample with no flash anneal. The right panel shows the PE loops for the millisecond flash annealed samples with varying flash energy density. In each case, there was a 120 s preheat step at 375 °C and the flash pulse duration was 20 ms.

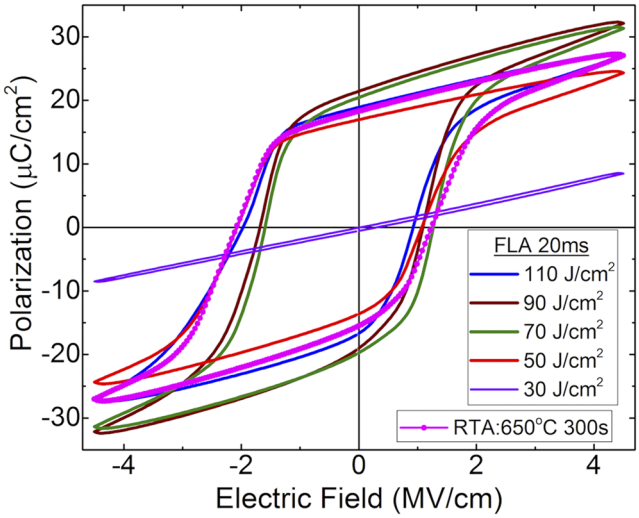

FIG. 5. Polarization versus electric field (PE) characteristics measured on W/TiN/HZO/TiN/n$^+$Si MIM structures at room temperature and at 1 kHz. Hysteresis loops (post cycling) are shown for the 300 s 650 °C *RTA* sample with no flash anneal and for the millisecond flash annealed samples with varying flash energy density. In regard to the latter, there was a 120 s preheat step at 375 °C and the flash pulse duration was 20 ms.

wake-up effect observed previously for various ferroelectric films.[20–23] In all ferroelectric samples, an imprint can be observed, whose origin is not yet clarified.

For ease of comparison, Fig. 5 plots the PE hysteresis loops measured post-cycling for the various *ms-FLA* samples and the 300 s 650 °C *RTA* sample. Two of the critical parameters in evaluating the quality of a ferroelectric layer are the coercive field strength (E_c) and the remanent polarization (P_r). In this regard, the 90 J/cm^2 and 70 J/cm^2 *ms-FLA* samples exhibit the highest P_r values (~21 μC/cm^2). E_c is ~1.1 MV/cm, and the 70 J/cm^2 sample exhibits slightly lower imprint. It is noted that the peaks observed previously in the CV curves for these samples in Fig. 3 coincide with these E_c values. The P_r and E_c values for the optimized *ms-FLA* samples in this study are comparable with those reported previously for HZO films of similar thickness.[8,11,13] While E_c is similar for the 300 s 650 °C *RTA* sample, the P_r values (~18 μC/cm^2) are lower than those observed for the optimized *ms-FLA* samples.

Another clear difference between the *RTA* and *ms-FLA* annealing is visible in endurance measurements (Fig. 6). A bipolar cycling with an amplitude of 3.5 V and a frequency of 1 kHz was applied

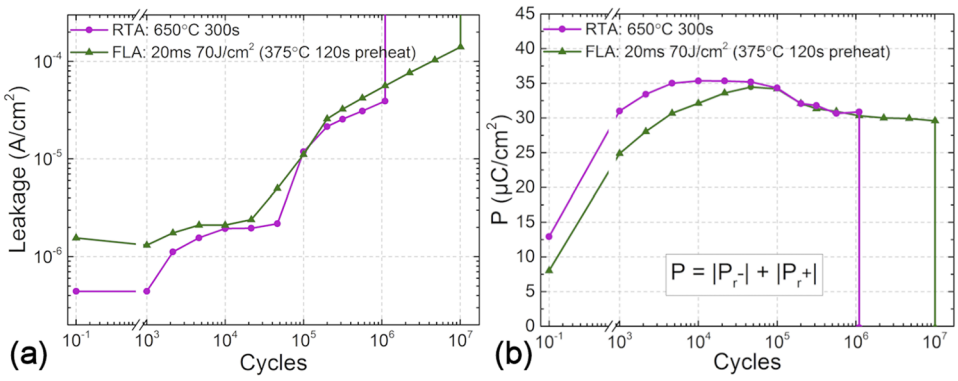

FIG. 6. Endurance characteristics measured on the 70 J/cm^2 *ms-FLA* and 300 s 650 °C *RTA* sample at room temperature. Bipolar cycling stress with an AC amplitude of 3.5 V and a frequency of 1 kHz up to 10^5 cycles and 100 kHz up to 10^7 cycles was applied. (a) DC leakage measured at 1 MV/cm. (b) Polarization extracted from PUND measurements with an amplitude of 4 V and a pulse width of 1 ms.

to both a 70 J/cm^2 *ms-FLA* sample and a 300 s 650 °C *RTA* sample up to 10^5 cycles. Afterwards, a frequency of 100 kHz was applied up to 10^7 cycles. Figure 6(a) shows the change in DC leakage, while Fig. 6(b) shows the evolution of the polarization (P) with cycling. Due to leakage current, P was determined by PUND measurements.[24] Three distinct regimes can be identified in both samples. First, P increases due to the wake-up effect until it reaches its maximum value of 35 μC/cm^2 at ~46 000 cycles. Applying more cycles result in a decrease in P accompanied by an increase in the leakage current. This regime is characteristic of the fatigue of the ferroelectric.[25] Finally, dielectric breakdown is reached at a number of cycles which determine the "endurance" of the material. The endurance of the 70 J/cm^2 *ms-FLA* sample is one order of magnitude higher than that for the 300 s 650 °C *RTA* sample [Fig. 6(b)]. At the same time, the wake-up of the 70 J/cm^2 *ms-FLA* sample is slower but reaches a comparable P maximum, whereas the fatigue process appears similar in both samples. The wake-up process can be attributed to the redistribution of existing defects such as oxygen vacancies[25,26] or phase transitions[25,27,28] in the device. The fatigue process on the other hand is a result of dielectric degradation due to an increasing trap density and domain pinning.[25,29] The slower wake-up phase is consistent with a delayed breakdown in *ms-FLA* films and can be attributed to a different microstructure obtained using the different anneal processes. The improved endurance illustrates the potential of using fast annealing to stabilize the FE phase of HZO in non-volatile memory elements.

In summary, ferroelectric behavior was demonstrated for ~10 nm $Hf_{0.57}Zr_{0.43}O_2$ films using a 120 s 375 °C pre-heat combined with a 20 ms flash lamp annealing pulse. The ferroelectric characteristics achieved using the *ms-FLA* were comparable to that obtained using a much higher thermal budget 300 s *RTA* at 650 °C, as confirmed using XRD, CV, PE, and endurance analyses. While a similar coercive field (~1.1 MV/cm) is achieved for both the *ms-FLA* and *RTA*, superior remanent polarization values are obtained for the optimized *ms-FLA* samples (~21 μC/cm^2) compared to the *RTA* sample (18 μC/cm^2) in this study. The increased endurance of the *ms-FLA* sample further emphasizes the advantage of the millisecond flash lamp annealing technique. Given the annealing temperature profile is one of the most critical factors for formation and stabilization of the ferroelectric orthorhombic phase in HZO, this millisecond FLA technique offers a promising low thermal budget alternative for crystallization of ferroelectric HZO films.

This project has received funding from the European Commission under Grant Agreement Nos. FP7-ICT 619325 (COMPOSE3) and H2020-ICT 688282 (PETMEM) and 780997 (plaCMOS) from the Swiss State Secretariat for Education and from Research and Innovation under Contract No. 16.0001. The authors would also like to thank Professor Adrian Ionescu of EPFL (École Polytechnique Fédérale de Lausanne).

[1] T. S. Böscke, J. Müller, D. Bräuhaus, U. Schröder, and U. Böttger, Appl. Phys. Lett. **99**, 102903 (2011).
[2] J. Muller, P. Polakowski, S. Mueller, and T. Mikolajick, ECS J. Solid State Sci. Technol. **4**, N30 (2015).
[3] M. H. Park, Y. H. Lee, H. J. Kim, Y. J. Kim, T. Moon, K. Do Kim, J. Müller, A. Kersch, U. Schroeder, T. Mikolajick, and C. S. Hwang, Adv. Mater. **27**, 1811 (2015).
[4] T. Olsen, U. Schröder, S. Müller, A. Krause, D. Martin, A. Singh, J. Müller, M. Geidel, and T. Mikolajick, Appl. Phys. Lett. **101**, 082905 (2012).
[5] S. Mueller, C. Adelmann, A. Singh, S. Van Elshocht, U. Schroeder, and T. Mikolajick, ECS J. Solid State Sci. Technol. **1**, N123 (2012).
[6] T. Schenk, S. Mueller, U. Schroeder, R. Materlik, A. Kersch, M. Popovici, C. Adelmann, S. Van Elshocht, and T. Mikolajick, in *2013 Proceedings of European Solid State Device Research Conference* (IEEE, 2013), pp. 260–263.
[7] J. Muller, T. S. Boscke, S. Muller, E. Yurchuk, P. Polakowski, J. Paul, D. Martin, T. Schenk, K. Khullar, A. Kersch, W. Weinreich, S. Riedel, K. Seidel, A. Kumar, T. M. Arruda, S. V. Kalinin, T. Schlosser, R. Boschke, R. van Bentum, U. Schroder, and T. Mikolajick, in *2013 IEEE International Electron Devices Meeting* (IEEE, 2013), pp. 10.8.1–10.8.4.
[8] J. Müller, T. S. Böscke, U. Schröder, S. Mueller, D. Bräuhaus, U. Böttger, L. Frey, and T. Mikolajick, Nano Lett. **12**, 4318 (2012).
[9] P. Polakowski and J. Müller, Appl. Phys. Lett. **106**, 232905 (2015).
[10] M. Hyuk Park, H. Joon Kim, Y. Jin Kim, W. Lee, T. Moon, and C. Seong Hwang, Appl. Phys. Lett. **102**, 242905 (2013).
[11] H. J. Kim, M. H. Park, Y. J. Kim, Y. H. Lee, T. Moon, K. Do Kim, S. D. Hyun, and C. S. Hwang, Nanoscale **8**, 1383 (2016).
[12] J. Müller, T. S. Böscke, D. Bräuhaus, U. Schröder, U. Böttger, J. Sundqvist, P. Kücher, T. Mikolajick, and L. Frey, Appl. Phys. Lett. **99**, 112901 (2011).
[13] A. Chouprik, S. Zakharchenko, M. Spiridonov, S. Zarubin, A. Chernikova, R. Kirtaev, P. Buragohain, A. Gruverman, A. Zenkevich, and D. Negrov, ACS Appl. Mater. Interfaces **10**, 8818 (2018).

[14] W. Skorupa, R. A. Yankov, M. Voelskow, W. Anwand, D. Panknin, R. A. McMahon, M. Smith, T. Gebel, L. Rebohle, R. Fendler, and W. Hentsch, in *2005 13th International Conference on Advanced Thermal Processing of Semiconductors* (IEEE, 2005), pp. 53–71.
[15] F. Ambriz-Vargas, G. Kolhatkar, M. Broyer, A. Hadj-Youssef, R. Nouar, A. Sarkissian, R. Thomas, C. Gomez-Yáñez, M. A. Gauthier, and A. Ruediger, ACS Appl. Mater. Interfaces **9**, 13262 (2017).
[16] P. Patsalas, N. Kalfagiannis, and S. Kassavetis, Materials **8**, 3128 (2015).
[17] M. N. Solovan, V. V. Brus, E. V. Maistruk, and P. D. Maryanchuk, Inorg. Mater. **50**, 40 (2014).
[18] H. Habuka, A. Hara, T. Karasawa, and M. Yoshioka, Jpn. J. Appl. Phys., Part 1 **46**, 937 (2007).
[19] S. Mueller, J. Muller, U. Schroeder, and T. Mikolajick, IEEE Trans. Device Mater. Reliab. **13**, 93 (2013).
[20] U. Schroeder, E. Yurchuk, J. Müller, D. Martin, T. Schenk, P. Polakowski, C. Adelmann, M. I. Popovici, S. V. Kalinin, and T. Mikolajick, Jpn. J. Appl. Phys., Part 2 **53**, 08LE02 (2014).
[21] D. Zhou, J. Xu, Q. Li, Y. Guan, F. Cao, X. Dong, J. Müller, T. Schenk, and U. Schröder, Appl. Phys. Lett. **103**, 192904 (2013).
[22] T. Schenk, U. Schroeder, M. Pešić, M. Popovici, Y. V. Pershin, and T. Mikolajick, ACS Appl. Mater. Interfaces **6**, 19744 (2014).
[23] K. Carl and K. H. Hardtl, Ferroelectrics **17**, 473 (1977).
[24] K. M. Rabe, M. Dawber, C. Lichtensteiger, C. H. Ahn, and J.-M. Triscone, *Physics of Ferroelectrics* (Springer Berlin Heidelberg, Berlin, Heidelberg, 2007), pp. 1–30.
[25] M. Pešić, F. P. G. Fengler, L. Larcher, A. Padovani, T. Schenk, E. D. Grimley, X. Sang, J. M. LeBeau, S. Slesazeck, U. Schroeder, and T. Mikolajick, Adv. Funct. Mater. **26**, 4601 (2016).
[26] S. Starschich, S. Menzel, and U. Böttger, Appl. Phys. Lett. **108**, 032903 (2016).
[27] M. H. Park, H. J. Kim, Y. J. Kim, Y. H. Lee, T. Moon, K. Do Kim, S. D. Hyun, and C. S. Hwang, Appl. Phys. Lett. **107**, 192907 (2015).
[28] P. D. Lomenzo, Q. Takmeel, C. Zhou, C. M. Fancher, E. Lambers, N. G. Rudawski, J. L. Jones, S. Moghaddam, and T. Nishida, J. Appl. Phys. **117**, 134105 (2015).
[29] M. Pesic, F. P. G. Fengler, S. Slesazeck, U. Schroeder, T. Mikolajick, L. Larcher, and A. Padovani, in *2016 IEEE International Reliability Physics Symposium* (IEEE, 2016), pp. MY-3-1–MY-3-5.